BIOCHEMISTRY
including biophysical chemistry & molecular biology

Article

pubs.acs.org/biochemistry

Functional Chimeras of GLIC Obtained by Adding the Intracellular Domain of Anion- and Cation-Conducting Cys-Loop Receptors

Nelli Mnatsakanyan,[†,‡,@] Sita Nirupama Nishtala,[†,‡] Akash Pandhare,[†,‡] Mariana C. Fiori,[†,‡] Raman Goyal,[†,‡] Jonathan E. Pauwels,[†,‡,§] Andrew F. Navetta,[†,∥] Afzal Ahrorov,[†,⊥] and Michaela Jansen*[,†,‡]

[†]Department of Cell Physiology and Molecular Biophysics, School of Medicine, Texas Tech University Health Sciences Center, Lubbock, Texas 79430, United States

[‡]Center for Membrane Protein Research, School of Medicine, Texas Tech University Health Sciences Center, Lubbock, Texas 79430, United States

[§]Center for Biotechnology and Genomics, Texas Tech University, Lubbock, Texas 79430, United States

[∥]Medical Student Summer Research Program, School of Medicine, Texas Tech University Health Sciences Center, Lubbock, Texas 79430, United States

[⊥]Undergraduate Science Education Program of the Howard Hughes Medical Institute, Texas Tech University, Lubbock, Texas 79430, United States

ABSTRACT: Pentameric ligand-gated ion channels (pLGICs), also called Cys-loop receptors in eukaryotic superfamily members, play diverse roles in neurotransmission and serve as primary targets for many therapeutic drugs. Structural studies of full-length eukaryotic pLGICs have been challenging because of glycosylation, large size, pentameric assembly, and hydrophobicity. X-ray structures of prokaryotic pLGICs, including the *Gloeobacter violaceus* LGIC (GLIC) and the *Erwinia chrysanthemi* LGIC (ELIC), and truncated eukaryotic pLGICs have significantly improved and complemented the understanding of structural details previously obtained with acetylcholine-binding protein and *Torpedo* nicotinic acetylcholine receptors. Prokaryotic pLGICs share their overall structural features with eukaryotic pLGICs for the ligand-binding extracellular and channel-lining transmembrane domains. The large intracellular domain (ICD) is present only in eukaryotic members and is characterized by a low level of sequence conservation and significant variability in length (50−250 amino acids), making the ICD a potential target for the modulation of specific pLGIC subunits. None of the structures includes a complete ICD. Here, we created chimeras by adding the ICD of cation-conducting (nAChR-α7) and anion-conducting (GABAρ1, Glyα1) eukaryotic homopentamer-forming pLGICs to GLIC. GLIC−ICD chimeras assemble into pentamers to form proton-gated channels, as does the parent GLIC. Additionally, the sensitivity of the chimeras toward modulation of functional maturation by chaperone protein RIC-3 is preserved as in those of the parent eukaryotic channels. For a previously described GLIC−5HT$_{3A}$−ICD chimera, we now provide evidence of its successful large-scale expression and purification to homogeneity. Overall, the chimeras provide valuable tools for functional and structural studies of eukaryotic pLGIC ICDs.

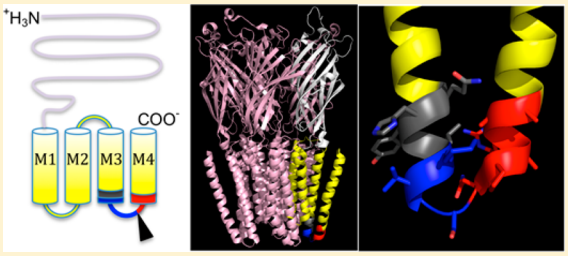

Cys-loop receptors or more broadly pentameric ligand-gated ion channels (pLGICs) are neurotransmitter-activated receptors selective for either cations or anions. They include cationic nicotinic acetylcholine (nACh) and serotonin (5-HT$_3$) receptors,[1,2] as well as anionic γ-aminobutyric acid type A (GABA$_A$), and glycine (GlyR) receptors.[3,4] This large superfamily is abundant in the central nervous system and conclusively contributes to many neurological diseases, conditions, and psychological behaviors, including anxiety and depression,[5] autism,[6] schizophrenia,[7] Parkinson's and Alzheimer's diseases,[8] epilepsy,[9] and nicotine addiction.[10]

High-resolution structural information for the N-terminal extracellular domain (ECD) of pLGIC was first obtained by X-ray crystallography of the ECD-homologous soluble protein acetylcholine-binding protein (AChBP).[11−13] The cryo-electron microscopy-derived *Torpedo* nAChR model additionally resolved the transmembrane domain (TMD) consisting of four α-helical segments, M1−M4,[14] and one cytosolic α-helical segment preceding M4, the so-called membrane-associated (MA) helix or amphipathic helix (HA).[15] After 15 putative homologues were computationally identified in prokaryotes in 2005,[16] higher-resolution X-ray structures of free and ligand-bound prokaryotic pLGICs were determined for the *Gloeobacter violaceus* LGIC, GLIC, and the *Erwinia chrysanthemi*

Received: December 15, 2014
Revised: April 6, 2015
Published: April 10, 2015

DOI: 10.1021/acs.biochem.5b00203
Biochemistry 2015, 54, 2670−2682

(syn. *Dickeya dadantii* or *Pectobacterium chrysanthemi*)[17] LGIC, ELIC.[18−25] Only eukaryotic members possess an intracellular domain (ICD) between M3 and M4. Prokaryotes instead have a 3−10-amino acid residue linker. Recently, eukaryotic pLGIC constructs that lack the ICD were engineered (GluClα and GABA$_A\beta$3) or that have the ICD proteolyzed were obtained, and their X-ray structures were determined.[26−28] The more recent structures inspired an experimental verification of the vertical alignment between M2 and M3 in nAChR, indicating a shift in register by two helical turns between M2 and M3 compared to the cryo-EM structural model.[26,29] Overall, all structures demonstrate the structural conservation of ECDs and TMDs. However, none of the X-ray structures of pLGICs contains the complete ICD that is by far the most diverse domain between different subtypes, with regard to both length and sequence conservation.[30]

Here, we describe chimeras obtained by inserting eukaryotic ICDs between M3 and M4 in GLIC. Specifically, we chose both cation-conducting and anion-conducting pLGICs that can form functional homopentamers to facilitate our studies. The eukaryotic ICDs of 75−145 amino acids were from cationic nAChα7, and from anionic GABA$_A\rho$1 and Glyα1. For each of the three ICDs, 12 different GLIC−eukaryotic−ICD chimeras were generated. Two-electrode voltage-clamp experiments after heterologous expression in *Xenopus laevis* oocytes identified functional chimeras that have functional characteristics similar to those of wild-type GLIC. Similarly, we have generated and characterized the corresponding GLIC−5-HT$_{3A}$−ICD chimeras containing the ICD of cation-conducting 5-HT$_{3A}$R previously described.[31] Additionally, we have investigated channel block by tetrabutylammonium (TBA) for all four chimera sets in this study. Importantly, we show now that functional GLIC−5-HT$_{3A}$−ICD chimeras can be expressed and purified as pentamers from *Escherichia coli*. This demonstrates that the GLIC−eukaryotic−ICD chimeras are amenable to large-scale expression and mass production, which makes them promising candidates for the study of the structure and function of the intracellular domain of Cys-loop receptors.

EXPERIMENTAL PROCEDURES

Plasmids. Human RIC-3 (hRIC-3) in the pGEMH19 expression vector was a generous gift of M. Treinin (The Hebrew University of Jerusalem, Jerusalem, Israel). Mouse 5-HT$_{3A}$ and human GABA$_A\rho$1 were generous gifts from M. Akabas (Albert Einstein College of Medicine, Bronx, NY); human nAChRα7 was a gift from J. Lindstrom (University of Pennsylvania, Philadelphia, PA), and rat Glyα1 was a gift from L. Sivilotti (University College London, London, U.K.). GABA$_A\rho$1 was previously termed GABA$_C\rho$1; however, we use the updated nomenclature.[32] The GLIC gene was amplified by polymerase chain reaction (PCR) out of a *G. violaceus* culture (ATCC 29082) and introduced into the pXOON vector as described previously.[31] A C-terminal FLAG epitope tag was inserted into GLIC utilizing PCR. The sequence for AflII and BsrGI restriction sites was introduced inside GLIC at the apex of the M3−M4 linker as seen in the X-ray structures (HYLKVES-insert-QPARAA) by PCR. These two restriction sites were used to ligate the mouse 5-HT$_{3A}$−ICD fragment (QDL QRP VP···RDW LRV GY) to obtain GLIC−5-HT$_{3A}$−ICD−AlB. For the generation of the GLIC−Glyα1−ICD−AlB, GLIC−GABA$_A\rho$1−ICD−AlB, and GLIC−nAChα7−ICD−AlB chimeras, homologous sequences for each ICD were ligated similarly into the GLIC linker. Subsequently, to optimize the insertion points of the ICD, the flanking regions of GLIC both N- and C-terminal to the inset were altered stepwise, yielding 11 additional chimeric GLIC−5-HT$_{3A}$−ICD, GLIC−Glyα1−ICD, GLIC−GABA$_A\rho$1−ICD, and GLIC−nAChα7−ICD constructs. Similarly, 12 chimeras were generated for each GLIC−eukaryotic−ICD set in bacterial expression the vector pET26b (Novagen). All constructs were verified by DNA sequencing (Genewiz, South Plainfield, NJ) of the complete coding region.

Oocyte Expression. GLIC chimera pXOON plasmids were linearized with XbaI or NheI, and the hRIC-3 pGEMH19 plasmid was linearized with NheI for *in vitro* transcription using T7 RNA polymerase (mMESSAGE mMACHINE kit, Applied Biosystems/Ambion, Austin, TX). Capped cRNA was purified with the MEGAclear kit (Applied Biosystems/Ambion) and precipitated with ammonium acetate. cRNA was dissolved in nuclease-free water and stored at −80 °C. The integrity of the cRNA was tested by agarose gel electrophoresis. *X. laevis* oocytes were harvested and defolliculated as described previously.[31] Unless otherwise noted, oocytes were injected 24 h after isolation with 10 ng of ion channel cRNA (0.2 μg/μL), with or without hRIC-3 cRNA (5 ng), and kept in standard oocyte saline medium {SOS [100 mM NaCl, 2 mM KCl, 1 mM $MgCl_2$, 1.8 mM $CaCl_2$, and 5 mM HEPES (pH 7.5)]} supplemented with 1% antibiotic-antimycotic (100×) and 5% horse serum for up to 7 days at 17 °C.

Oocyte Two-Electrode Voltage-Clamp (TEVC) Experiments. TEVC experiments were conducted 2−5 days after cRNA injection at a holding potential of −60 mV and room temperature. A ∼250 μL chamber harboring a single oocyte was continuously perfused at a rate of 5−6 mL/min with GLIC oocyte recording buffer {GORB [100 mM NaCl, 20 mM NaOH, 2.5 mM KCl, 1 mM $MgCl_2$, 2 mM $CaCl_2$, 5 mM HEPES, and 5 mM citric acid (pH adjusted to 7.5 or as indicated with HCl)]}. The ground electrode was connected to the bath by a 3 M KCl/agar bridge. The glass microelectrode resistance was <2 MΩ when the system was filled with 3 M KCl. Data were acquired and analyzed using a TEV-200 amplifier (Dagan Instruments, Minneapolis, MN), a Digidata 1440A data interface (Molecular Devices, Sunnyvale, CA), and pClamp 10.2 software (Molecular Devices). Currents (I_{pH}) elicited by lowering the pH of GORB below 7.5 were separated by a GORB (pH 7.5) wash for 6 min for the oocytes to recover from desensitization. Currents were considered to be stable if the variation between consecutive I_{pH} values varied by ≤10−15%. All experiments were performed on at least three oocytes from two different batches of oocytes.

Functional Screening of Chimeras. Initially, the macroscopic functionality of all chimeras was assayed by using TEVC by measuring the proton-induced current amplitude induced by changing the extracellular pH from 7.5 to 5.

Proton Concentration for Determination of Half-Maximal Activation (pH_{50}). Proton concentration−response curves were obtained by exposing the oocytes to GORB at pH <7.5 until a steady-state current was reached for the respective pH and switching back to GORB (pH 7.5). Currents were normalized to the maximal current obtained for each oocyte. Most oocytes tolerated pH 4, and currents returned rapidly to the initial baseline when the pH was switched back to 7.5. Oocytes that became unstable upon exposure to acidic pH (5−10%) were eliminated from data analysis. No significant currents were obtained in mock oocytes (water-injected or uninjected). At pH 4, the current in mock oocytes was <100

DOI: 10.1021/acs.biochem.5b00203
Biochemistry 2015, 54, 2670−2682

nA, which was ≤10% of what was recorded in functional GLIC constructs at the same pH. Data were fit using GraphPad Prism version 6.00 (GraphPad Software, La Jolla, CA) with the equation

$$\text{percent activation} = 100/[1 + 10^{(\log EC_{50} - \log[H^+])n_H}]$$

where $[H^+]$ is the proton concentration, n_H is the Hill coefficient, and EC_{50} is the H^+ concentration for half-maximal activation. The pH at half-maximal activation (pH_{50}) is calculated as follows

$$pH_{50} = -\log EC_{50}$$

Parameters from several oocytes were averaged to obtain the mean EC_{50} and Hill coefficient. Data are presented as means ± the standard error of the mean (SEM).

Concentration of TBA That Induces Half-Maximal Inhibition (IC_{50}) Determination. Large quaternary ammonium compounds act as open channel blockers of nAChR, and also of GLIC, by binding inside the channel pore roughly halfway across the membrane.[33] To compare the channel morphology of our chimeras with that of GLIC, we investigated channel block by TBA.[33] A stock of 1 M TBA (Sigma-Aldrich) in nuclease-free water was prepared on the day of the experiment, and dilutions were made before each experiment in GORB at pH 4.5. Inhibition curves were obtained by first superfusing the oocyte at pH 7.5 and then exposing it to an initial pH of 4.5. Once a steady-state current was reached, a dilution of TBA (0.1 μM to 10 mM at pH 4.5) was applied. Upon stabilization of this current, the reversibility of block was tested by application of GORB at pH 4.5 without TBA. When the steady-state current was reached, the currents were allowed to return to baseline by application of GORB at pH 7.5. This procedure was repeated for different concentrations of TBA to obtain the IC_{50} curve. Currents obtained in the presence of TBA were normalized against the current obtained for the pH 4.5 application alone for each individual oocyte. Data were fit with Prism using the following equation:

$$\text{percent current remaining} = 100/[1 + 10^{(\log IC_{50} - X) \times n_H}]$$

Co-expression of hRIC-3 with GLIC−Eukaryotic−ICD Chimeras. *X. laevis* oocytes were co-injected with cRNAs of hRIC-3 (5 ng) and wild-type GLIC (10 ng) or functional GLIC−nAChα7−ICD, GLIC−Glyα1−ICD, and GLIC−$GABA_A\rho$1−ICD chimeras (10 ng). We investigated the effect of hRIC-3 on receptor expression levels by measuring the current amplitudes with two-electrode voltage-clamp recordings by switching the pH of the external buffer from 7.5 to 5.0.

Immunoblotting. Oocytes, injected with Glyα1 wild-type cRNA, as well as with GLIC−Glyα1−ICD 1B, 0B, 2A, 2B, AlB, and 0 mutant cRNAs were washed thrice with OR2 (oocyte recording buffer 2) on the day of the experiment and then reacted with 0.5 mg/mL sulfo-NHS-LC-biotin (Thermo Scientific) in OR2 (pH 7.5) for 30 min, after which they were washed thrice with 1× OR2. Oocytes were then incubated for 10 min at room temperature with buffer H [20 mM Tris-HCl (pH 7.4) and 100 mM NaCl], followed by incubation with buffer H++ [buffer H with 1% Triton X-100 and 0.5% sodium deoxycholate and protease inhibitors (Thermo Scientific)]. They were then triturated and incubated for 1−2 h. High Capacity NeutrAvidin Agarose beads (Thermo Scientific) were washed with buffer H+ (buffer H with 1% Triton X-100 and 0.5% sodium deoxycholate). Solubilized oocytes were centrifuged twice at 20000*g* for 10 min at 4 °C. The clear middle layer from each spin was separated, combined, and added to the washed NeutrAvidin beads, and the entire mixture was allowed to rotate at 4 °C for 1−2 h; 90 μL of the clear middle layer between the yolk and pellet was kept as a total protein fraction. Total protein was separated from biotinylated plasma membrane proteins by centrifuging the NeutrAvidin bead lysate mixture at 2500*g* for 2 min. The pellet was then washed thrice with buffer H++. Laemmli buffer (4× SDS sample buffer) was added to the samples, and the samples were incubated at 37 °C for 10 min and then loaded onto a 4 to 15% TGX gel (Bio-Rad Laboratories), blotted to PVDF membranes (Bio-Rad Laboratories), and probed with goat anti-Glyα1 primary antibody (Everest Biotech) and rabbit anti-goat HRP-conjugated secondary antibody (Thermo Scientific). Blots were then developed with enhanced chemoluminescence substrate (Thermo Scientific).

Overexpression and Purification of GLIC−Eukaryotic−ICD Chimeras. Wild-type GLIC and GLIC−5-HT_{3A}−ICD 1B and 0B chimeric proteins were cloned into prokaryotic expression vector pET26b and expressed as a fusion construct with N-terminal maltose-binding protein (MBP) as described previously.[19,31] Wild-type GLIC and chimeric proteins were overexpressed in *E. coli* C41 cells,[34] grown in Terrific Broth medium, containing 50 μg/mL kanamycin at 37 °C to an A_{600} of ∼1.6−1.8. Expression was induced with 0.2 mM isopropyl β-D-thiogalactopyranoside overnight at 20 °C. Cells were harvested and lysed using a *microfluidizer* (Microfluidics, Inc.) in 50 mM potassium phosphate buffer with 150 mM NaCl (pH 8.0) (buffer A), with protease inhibitors. Unbroken cells were removed from the cell lysate by centrifugation (20 min at 10000*g*), and the membranes were isolated by ultracentrifugation (60 min at 100000*g*). The proteins were extracted from membranes with 2% *n*-dodecyl β-D-maltoside (DDM, Anatrace) under agitation at 4 °C, and the solubilized fraction was cleared by ultracentrifugation. Solubilized proteins were first purified by affinity chromatography, by binding to a Ni-NTA column (Qiagen). The maltose-binding protein tag was cleaved with human rhinovirus (HRV) 3C protease (Sino Biological Inc., Beijing, China). Wild-type GLIC and GLIC chimeric proteins were then separated from the cleaved His_{10}-MBP tag by using size exclusion chromatography on a Superdex 200 10/300 size exclusion column (SEC, GE Healthcare) equilibrated with buffer A with 0.05% DDM.

Gel Filtration Chromatography of GLIC−5-HT_{3A}−ICD 1B. The oligomeric state of GLIC−5-HT_{3A}−ICD 1B was assessed by refractionating the peak from a first SEC by gel filtration chromatography on a Superdex 200 10/300 size exclusion column that was equilibrated with buffer A with 0.05% DDM. The eluate was monitored by UV absorbance at 280 nm. The apparent molecular mass of GLIC−5-HT_{3A}−ICD 1B was determined by using the elution positions of molecular mass standards, resolved under identical buffer conditions. The elution volumes were as follows: ovalbumin (44 kDa), 15.4 mL; conalbumin (75 kDa), 14.6 mL; aldolase (158 kDa), 13.2 mL; ferritin (440 kDa), 10.8 mL. The calculated molecular mass of a single subunit for the GLIC−5-HT_{3A}−ICD 1B chimera based on its amino acid sequence is 49 kDa, and for the pentamer 245 kDa.

Dynamic Light Scattering of GLIC−5-HT_{3A}−ICD 1B. The oligomeric state of highly purified GLIC−5-HT_{3A}−ICD 1B protein (peak collected from SEC) was also analyzed by dynamic light scattering measurements. Purified protein, in 50

DOI: 10.1021/acs.biochem.5b00203
Biochemistry 2015, 54, 2670−2682

mM potassium phosphate (pH 8.0), 150 mM NaCl, and 1 mM DDM, was diluted to a protein concentration of 1.0 mg/mL. Samples were filtered with a 0.22 um Millipore Millex-GV filter right before measurements, and the protein was subjected to the light scattering measurements at 90° using a Brookhaven Instruments (Brookhaven, CT) BI-200SM device with an avalanche photodetector. The molecular mass of the protein was calculated from the measured hydrodynamic radius and a calibration curve that included seven soluble proteins commonly used as molecular mass standards for size exclusion chromatography (ribonuclease A, carbonic anhydrase, bovine serum albumin, conalbumin, aldolase, ovalbumin, and IgG), and three membrane proteins (KcsA, connexin 26 hemichannels, and P-glycoprotein).

Microtransplantation of Purified GLIC−5-HT$_{3A}$−ICD 1B Chimeras into *X. laevis* Oocytes. Oocytes were injected with 100 ng of purified GLIC−5-HT$_{3A}$−ICD 1B chimera in 0.02% DDM and incubated overnight at 16 °C. Two-electrode voltage-clamp recordings were performed ∼16 h postinjection at a holding potential of −60 mV, as we described elsewhere,[35,36] with few modifications. Currents were elicited in response to switching perfusion buffer from pH 7.5 to 4.0. The oocyte chamber was continuously perfused with GORB at a rate of ∼5 mL/min.

RESULTS

Functional GLIC Channels Obtained by Inserting Different Eukaryotic ICDs into the GLIC M3−M4 Linker. We generated chimeras by engineering the ICDs from three different mammalian receptors, nAChα7, GABA$_A$ρ1, and Glyα1, into the GLIC channel. All chimeras contain the complete amino acid sequence of the respective mammalian ICDs, but for each ICD, a series of chimeras that differ in the portions of the GLIC M3−M4 linker that were removed in stepwise fashion was generated (Figure 1). Optimization of the insertion points of ICDs thus led to the construction of 12 different chimeras for each GLIC−eukaryotic−ICD set. In a previous study, we had found that only two of 12 chimeras for GLIC−5-HT$_{3A}$−ICD chimeras were functional.[31] Therefore, we decided to generate a similar series for each of the ICDs used in this study, with the intent of finding at least one functional chimera in each set. All 36 chimeras were heterologously expressed in *X. laevis* oocytes, and their functionality was tested by two-electrode voltage-clamp experiments. Because GLIC is a proton-gated channel,[37] the functionality of the generated chimeras with respect to their ability of being gated by protons was screened by measuring the current amplitudes induced by changing the extracellular pH from 7.5 to 5. At least 10 chimeras of 12 were found to be functional for each prokaryotic−eukaryotic−ICD set, with the current amplitudes significantly different from those of water-injected oocytes (Figure 2). For the GLIC−Glyα1−ICD set, 10 chimeras were functional with current amplitudes ranging from 2000 to 4000 nA. Eleven of the GLIC−nAChα7−ICD chimeras were functional, and the current amplitudes range from 4000 to 6000 nA. All 12 chimeras were functional in the GLIC−GABA$_A$ρ1−ICD chimera set with a range of current amplitudes from 4000 to 6000 nA.

Nonfunctional GLIC−Glyα1−ICD Chimeras Are Expressed on the Plasma Membrane. Two chimeras, 2A and 2B, from the GLIC−Glyα1−ICD set were nonfunctional. We tested plasma membrane expression levels of chimeras from the GLIC−Glyα1−ICD set by biotinylating membrane proteins

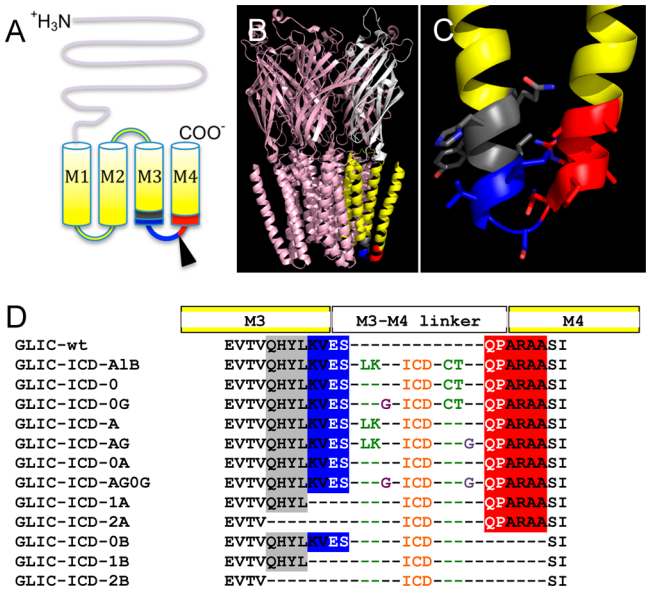

Figure 1. M3−M4 loop in GLIC and design of the chimeras. (A) Membrane topology of an individual GLIC subunit. The gray band represents the extracellular domain, and the yellow region the transmembrane domain with four α-helical segments (M1−M4); dark gray, blue, and red regions indicate the M3−M4 linker region. The triangle indicates the apex of the M3−M4 linker in the GLIC X-ray structure where the eukaryotic ICDs were inserted. (B) Schematic representation of GLIC (Protein Data Bank entry 3EAM) with regions color-coded as in panel A for one subunit; the other subunits are colored pink. (C) Magnification of the M3−M4 linker region. (D) Sequence comparison of the M3−M4 linker area for wild-type GLIC and engineered chimeras. Yellow bars on top indicate α-helical segments M3 and M4. Gray, blue, and red backgrounds indicate amino acids that were deleted from some linkers, where the respective areas are missing. Black letters indicate α-helical segments, white letters the wild-type GLIC M3−M4 linker residues, and green letters residues added because of the engineered restriction sites (LK for AflII and CT for BsrGI). Violet (G) indicates a Gly that was added for flexibility, and the orange ICD represents the location of the inserted ICD.

with membrane-impermeant sulfo-NHS-LC-biotin, isolating the biotinylated proteins with avidin beads, and subsequently performing Western blot analysis by using goat anti-Glyα1 primary and anti-goat HRP-conjugated secondary antibody. All tested constructs, including the two nonfunctional chimeras GLIC−Glyα1−ICD 2A and 2B were found in total protein as well as in plasma membrane protein fractions of oocytes (Figure 3). Our results indicate that the insertion of the 75-amino acid ICD from Glyα1 did not alter the cell surface expression of GLIC−Glyα1−ICD chimeras 2A and 2B. The somewhat smeared running behavior of the 2A and SB chimera bands as compared to that of other functional chimeras may indicate a slightly increased susceptibility to protease degradation. The results indicate that the nonfunctional chimeras are capable of assembly and trafficking to the plasma membrane. The loss of function of 2A and 2B constructs can perhaps be explained by defective folding, which may have interfered with either structural rearrangements underlying gating transitions of the ion channel pore or obstruction of the channel cavity.

The Proton Concentration That Induces Half-Maximal Activation of Chimeric Channels Is within an Order of Magnitude of That of Wild-Type GLIC. The concentration of agonist, in this case protons, that induces half-maximal

DOI: 10.1021/acs.biochem.5b00203
Biochemistry 2015, 54, 2670−2682

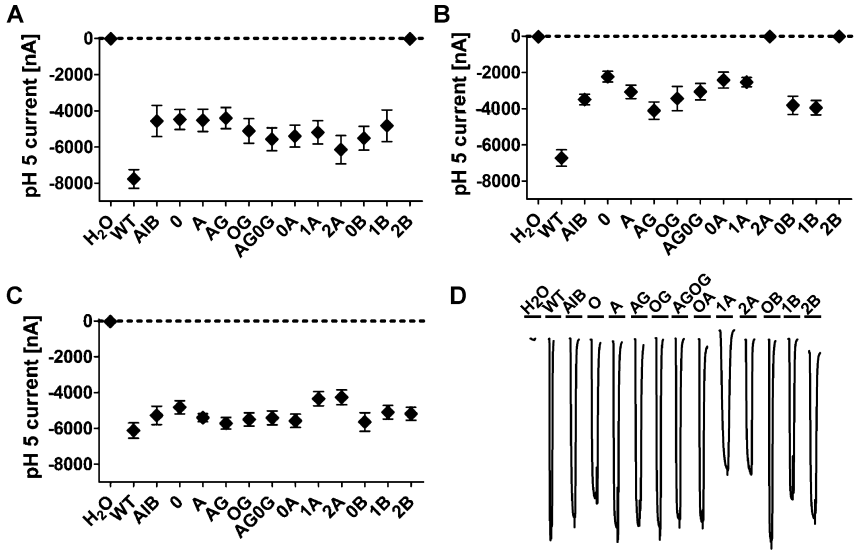

Figure 2. Screening for functional GLIC−eukaryotic−ICD chimeras after expression in *X. laevis* oocytes. Current amplitudes were recorded for (A) GLIC−nAChα7−ICD (11−23 oocytes per construct), (B) GLIC−Glyα1−ICD (5−8 oocytes per construct), and (C) GLIC−GABA$_A\rho$1−ICD (6−11 oocytes per construct) chimeras by switching the pH of the perfusion buffer from 7.5 to 5. (D) Sample currents obtained for GLIC−GABA$_A\rho$1−ICD chimeras. The membrane potential was held constant at −60 mV. *X. laevis* oocytes were injected with cRNA of wild-type GLIC or different GLIC−eukaryotic−ICD chimeras. All current amplitudes were compared with mock (uninjected or water-injected) oocytes by one-way analysis of variance with Dunnett's multiple-comparison post test. All symbols located off the dotted lines are significantly different from data of mock oocytes. For 11 GLIC−nAChα7−ICD chimeras (except 2B that was not significant) and all GLIC−GABA$_A\rho$1−ICD chimeras, the multiplicity-adjusted p value was <0.0001 upon comparison to mock oocytes; for GLIC-Glyα1-ICD, the 0 chimera had a p value of 0.0011, and for 0A and 1A, the p values were 0.0004 and 0.0002, respectively. 2A and 2B were not significant, and all others had p values of <0.0001. Error bars indicate SEM.

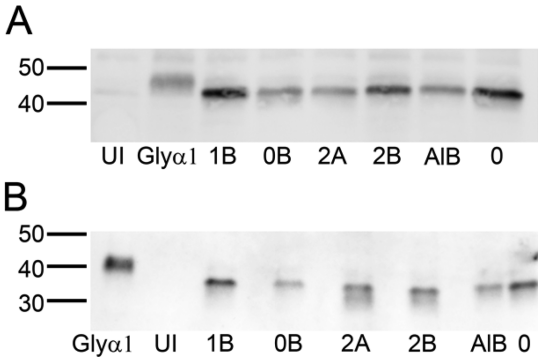

Figure 3. (A) Total and (B) plasmamembrane protein expression of GLIC−Glyα1−ICD chimeras in *X. laevis* oocytes. Plasma membrane proteins were isolated after biotinylation with sulfo-NHS-LC biotin and subsequent incubation with avidin beads. The plasma membrane and total protein fractions of oocytes were resolved on TGX gels, blotted to PVDF membranes, and probed with goat anti-Glyα1 antibody (Everest Biotech), and subsequently HRP-conjugated rabbit anti-goat antibody (Thermo Scientific). Glyα1 wild-type cRNA and water-injected oocytes (UI) were used as positive and negative controls, respectively. Note that all chimeras are detected in plasma membrane fractions, and that the nonfunctional chimeras 2A and 2B have the highest expression level.

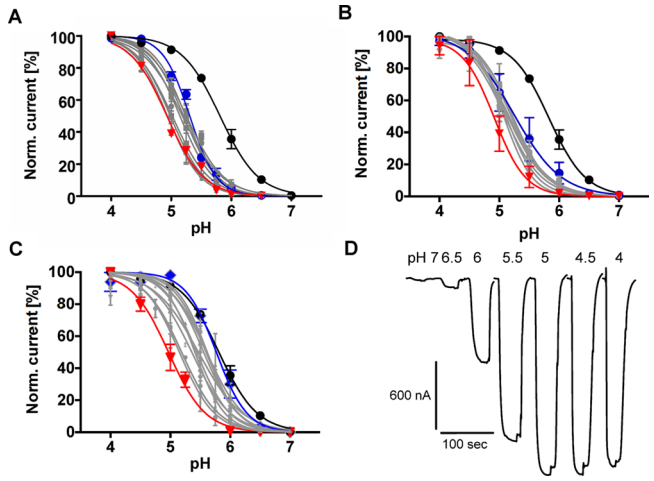

Figure 4. Dose−response relationships for proton gating of functional GLIC−eukaryotic−ICD chimeras: (A) GLIC−nAChα7−ICD, (B) GLIC−Glyα1−ICD, and (C) GLIC−GABA$_A\rho$1−ICD. (D) Sample current traces shown for GLIC−GABA$_A\rho$1−ICD 0B. Currents recorded by TEVC from *X. laevis* oocytes injected with wild-type GLIC (black symbols and black dose−response curve) and chimera cRNA (lowest pH$_{50}$ colored red, highest blue, and all others gray) obtained by graded reductions of perfusion buffer pH. The holding potential was −60 mV. Error bars indicate the SEM. Chimeras were compared to wild-type GLIC by one-way analysis of variance with Dunnett's multiple-comparison post test, and results are detailed in Tables 1−3.

activation (pH$_{50}$ = −log EC$_{50}$) of wild-type GLIC and chimeric channels was determined in TEVC experiments after expression in *X. laevis* oocytes. The results for pH$_{50}$ and Hill coefficient (n_H) values for all chimeras are summarized in Figure 4, as well as Tables 1−3. The pH$_{50}$ values of chimeric channels were compared to that of wild-type GLIC by using one-way analysis of variance with Dunnett's post hoc test and were found to be significantly different from that of wild-type GLIC (pH$_{50}$ = 5.8) for all the constructs from the GLIC−Glyα1−ICD and GLIC−nAChα7−ICD chimera sets. The chimeras with the most acidic pH$_{50}$ values are 1A (pH 4.89 and 4.87) for both the GLIC−Glyα1−ICD and GLIC−nAChα7−ICD sets (Figure 3). The chimeras with the most basic pH$_{50}$ values are 1B (pH 5.30) and AG (pH 5.32) for the GLIC−

DOI: 10.1021/acs.biochem.5b00203
Biochemistry 2015, 54, 2670−2682

Table 1. Comparison of the Log EC_{50} and Hill Coefficient Values of GLIC−Glyα1−ICD Chimeras with Wild-Type GLIC[a]

chimera	−log EC_{50}	n_H	n
WT GLIC	5.81 ± 0.05	−1.40 ± 0.10	3
O	5.07 ± 0.13[d]	−1.94 ± 0.22	6
A	5.16 ± 0.11[c]	−1.48 ± 0.16	3
OG	5.23 ± 0.07[b]	−1.63 ± 0.13	4
AG	5.20 ± 0.18[b]	−1.84 ± 0.06	3
OA	5.07 ± 0.04[c]	−1.85 ± 0.19	3
OB	5.18 ± 0.06[c]	−1.39 ± 0.02	3
1A	4.90 ± 0.16[d]	−2.15 ± 0.50	3
1B	5.30 ± 0.19[b]	−1.33 ± 0.05	3
AGOG	5.11 ± 0.03[c]	−1.73 ± 0.13	4
AlB	5.14 ± 0.05[c]	−1.47 ± 0.15	4

[a]Log EC_{50} and Hill coefficient (n_H) values of GLIC−Glyα1−ICD chimeras were compared to those of wild-type GLIC by one-way ANOVA with Dunnett's multiple-comparison post test. The number of oocytes per construct is given as n. Standard errors are given. [b]Multiplicity-adjusted p value of <0.05. [c]Multiplicity-adjusted p value of ≤0.01. [d]Multiplicity-adjusted p value of ≤0.001.

Table 2. Comparison of the Log EC_{50} and Hill Coefficient Values of GLIC−$GABA_A\rho$1−ICD Chimeras with Wild-Type GLIC[a]

chimera	−log EC_{50}	n_H	n
WT GLIC	5.81 ± 0.05	−1.40 ± 0.10	3
O	5.46 ± 0.24	−1.50 ± 0.17	3
A	5.55 ± 0.07	−1.60 ± 0.19	3
OG	5.60 ± 0.04	−1.62 ± 0.06	3
AG	5.19 ± 0.02[c]	−1.44 ± 0.11	3
OA	5.64 ± 0.14	−1.95 ± 0.37	3
OB	5.38 ± 0.05[b]	−1.40 ± 0.16	4
1A	4.94 ± 0.09[d]	−1.68 ± 0.07	4
1B	5.42 ± 0.12	−1.98 ± 0.45	3
2A	5.16 ± 0.05[c]	−1.59 ± 0.22	3
2B	5.77 ± 0.08	−1.81 ± 0.14	3
AGOG	5.46 ± 0.12	−1.62 ± 0.13	4
AlB	5.59 ± 0.14	−1.89 ± 0.31	3

[a]Log EC_{50} and Hill coefficient (n_H) values of GLIC−ICD chimeras were compared to those of wild-type GLIC by one-way ANOVA with Dunnett's multiple-comparison post test. The number of oocytes per construct is given as n. Standard errors are given. [b]Multiplicity-adjusted p value of <0.05. [c]Multiplicity-adjusted p value of ≤0.01. [d]Multiplicity-adjusted p value of ≤0.0001.

Glyα1−ICD and GLIC−nAChα7−ICD sets, respectively. There are only four constructs, AG, 1A, 2A, and 0B, in the GLIC−$GABA_A\rho$1−ICD chimera set with pH_{50} values significantly different from that of wild-type GLIC. The Hill coefficient (n_H) ranged from 1.3 to 2.2 and was not significantly different for any of the chimeras compared to that of wild-type GLIC (n_H = 1.4), except for GLIC−nAChα7−ICD AG (n_H = 1.9).

The Channel Blocker Concentration That Causes Half-Maximal Inhibition Is within an Order of Magnitude for Chimeras As Compared to That of Wild-Type GLIC. GLIC can be reversibly inhibited by quaternary ammonium compounds added to the extracellular side of the channel.[33] We investigated the inhibitory effect of a known GLIC blocker, TBA, on the chimeras by TEVC recordings in *X. laevis* oocytes injected with cRNA of wild-type GLIC and GLIC−eukaryotic−

Table 3. Comparison of the Log EC_{50} and Hill Coefficient Values of GLIC−nAChα7−ICD Chimeras with Wild-Type GLIC[a]

chimera	−log EC_{50}	n_H	n
WT GLIC	5.81 ± 0.05	−1.40 ± 0.10	3
O	5.23 ± 0.10[c]	−1.70 ± 0.12	3
A	5.20 ± 0.06[c]	−1.58 ± 0.08	3
OG	4.94 ± 0.03[c]	−1.57 ± 0.03	3
AG	5.31 ± 0.01[b]	−1.94 ± 0.12[d]	3
OA	4.93 ± 0.03[c]	−1.44 ± 0.08	3
OB	5.18 ± 0.12[c]	−1.41 ± 0.11	3
1A	4.93 ± 0.02[c]	−1.43 ± 0.04	3
1B	5.28 ± 0.08[b]	−1.38 ± 0.03	3
2A	5.02 ± 0.14[c]	−1.63 ± 0.07	3
AGOG	4.98 ± 0.002[c]	−1.53 ± 0.09	3
AlB	5.15 ± 0.06[c]	−1.59 ± 0.13	3

[a]Log EC_{50} and Hill coefficient (n_H) values of GLIC−ICD chimeras were compared to those of wild-type GLIC by one-way ANOVA with Dunnett's multiple-comparison post test. The number of oocytes per construct is given as n. Standard Errors are given. [b]Multiplicity-adjusted p value of ≤0.001. [c]Multiplicity-adjusted p value of ≤0.0001. [d]Multiplicity-adjusted p value of ≤0.01.

ICD chimeras. The half-maximal inhibitory concentration (IC_{50}) of TBA was determined for 1B and 0B chimeras from each set using a pH of 4.5 to open the channels. The IC_{50} and log IC_{50} values are summarized in Figure 5 and Table 4. The IC_{50} for wild-type GLIC was found to be 0.5 mM. The TBA IC_{50} values for the chimeras ranged from 0.1 to 2 mM. While both GLIC−Glyα1 and GLIC−nAChα7 chimeras displayed IC_{50} values similar to that of wild-type GLIC, both GLIC−$5HT_{3A}$ chimeras had a significantly lower IC_{50} (0.1 mM) and the GLIC−$GABA_A\rho$1 0B chimera a significantly higher IC_{50} (2 mM). The GLIC−$GABA_A\rho$1-1B chimera behaved like wild-type GLIC. Overall, compared to wild-type GLIC, the chimeras displayed IC_{50} values for TBA that were 5-fold lower to 4-fold higher than that of the wild type.

hRIC-3 Alters Plasma Membrane Expression of Chimeras That Contain the ICD of Cation-Conducting, but Not Anion-Conducting, Cys-Loop Receptors. hRIC-3 (resistance to inhibitors of cholinesterase) is a member of a conserved gene family that has been described as a chaperone protein that influences plasma membrane expression levels of various Cys-loop receptors such as nAChα7, nAChα4β2, and 5-HT_{3A} receptors by modulating maturation of these receptors.[38,39] We have previously shown that for 5-HT_{3A} receptors, the ICD is required for the attenuation of serotonin-induced currents observed upon co-expression with hRIC-3.[40] Additionally, we have demonstrated that current amplitudes caused by acidic gating (switch from pH 7.5 to 5) in GLIC−5-HT_{3A}−ICD chimeras 0B and 1B are attenuated when the chimeras are co-expressed with hRIC-3 in *X. laevis* oocytes.[31] On the contrary, hRIC-3 co-expression did not alter currents in wild-type GLIC-expressing oocytes. Here, we co-expressed hRIC-3 with GLIC−nAChα7−ICD, GLIC−$GABA_A\rho$1−ICD, and GLIC−Glyα1−ICD chimeras and recorded current amplitudes upon switching from external buffer at pH 7.5 to buffer at pH 5. Oocytes co-expressing GLIC−nAChα7−ICD chimeras show attenuated currents when they are co-expressed with hRIC-3 as compared with oocytes expressing only the chimeras (Figure 6). The mean current levels without RIC-3 ranged from 2744 to 5034 nA in all chimeras and from 34 to 466 nA in all

DOI: 10.1021/acs.biochem.5b00203
Biochemistry 2015, 54, 2670−2682

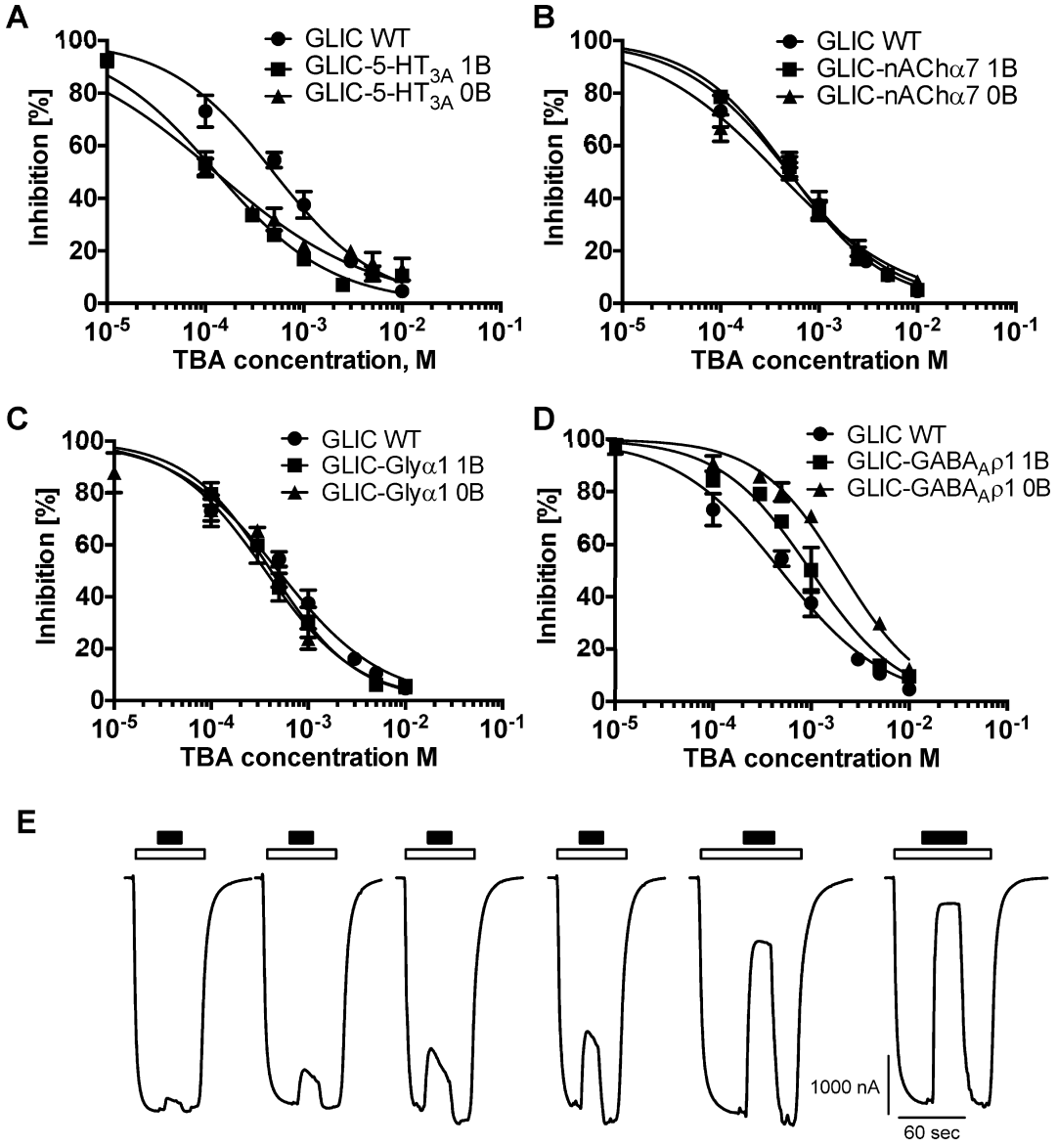

Figure 5. Dose–response relationships for inhibition by the channel blocker TBA in GLIC–eukaryotic–ICD chimeras: (A) GLIC–5-HT_{3A}–ICD, (B) GLIC–nAChα7–ICD, (C) GLIC–Glyα1–ICD, and (D) GLIC–$GABA_A$ρ1–ICD. (E) Current traces recorded from GLIC–$GABA_A$ρ1–ICD 0B provided as an example. Empty bars over current traces indicate the application period of pH 4.5 and filled bars of TBA at increasing concentrations. TEVC experiments were conducted in *X. laevis* oocytes injected with cRNA of wild-type GLIC (●) and different GLIC–eukaryotic–ICD chimeras [1B (■) and 0B (▲)]. The holding potential was −60 mV. Error bars indicate the SEM. Chimeras were compared to wild-type GLIC by one-way analysis of variance with Dunnett's multiple-comparison post test, and results are detailed in Table 4.

chimeras co-expressed with hRIC-3. After RIC-3 co-expression, currents were similar to those of mock oocytes. However, the current amplitudes of anionic–ICD chimeras, both GLIC–$GABA_A$ρ1–ICD and GLIC–Glyα1–ICD, were not altered by hRIC-3 co-expression (Figure 6). With regard to hRIC-3 interaction, the chimeras thus closely reflect the parent eukaryotic wild-type receptors that contributed the ICD to the chimeras, in that expression of 5-HT_{3A} and nAChα7 is altered by hRIC-3 whereas that of $GABA_A$ρ1 and Glyα1 is not changed.[38,39,41] This suggests that the ICD in both GLIC–nAChα7–ICD and GLIC–5-HT_{3A}–ICD chimeras interacts with hRIC-3, and that this interaction alters the level of expression of functional channels in the plasma membrane.

GLIC–5-HT_{3A}–ICD Chimeras Purified from *E. coli* Membranes Are Pentameric Assemblies. We expressed wild-type GLIC and the two functional chimeras from GLIC–5-HT_{3A}–ICD set, 1B and 0B, in *E. coli* as N-terminal fusion proteins with maltose-binding protein (MBP). *E. coli* membranes were solubilized with 2% DDM, and proteins were purified by Ni affinity chromatography (Figure 7A). The MBP tag was cleaved with human rhinovirus (HRV) 3C protease, and the GLIC chimeras were separated from cleaved His_{10}-MBP tags by using size exclusion chromatography (SEC) on a Superdex 200 10/300 column, equilibrated in buffer A with 0.05% DDM. Fractions of the peak corresponding to the pentamer were pooled and concentrated (Figure 7B). Molecular mass markers were used for generating a calibration for size determination with SEC (Figure 7C). The calculated molecular mass of pentameric GLIC–5-HT_{3A}–ICD 1B chimera, based on its amino acid sequence, is 245 kDa. On the basis of the elution volume of 11.96 ± 0.04 mL (n = 5), its size is 265.6 ± 5.1 kDa. The pentameric assembly of purified

DOI: 10.1021/acs.biochem.5b00203
Biochemistry 2015, 54, 2670–2682

Table 4. Log IC_{50} Values for TBA Inhibition of pH 4.5-Induced Currents[a]

chimera	log IC_{50}	IC_{50} (μM)	n
WT GLIC	−3.34 ± 0.10	525	6
GLIC−5-HT_{3A} 1B	−3.92 ± 0.07[b]	125	5
GLIC−5-HT_{3A} 0B	−4.02 ± 0.15[c]	120	6
GLIC−nAChα7 1B	−3.30 ± 0.08	525	4
GLIC−nAChα7 0B	−3.44 ± 0.10	392	4
GLIC−$GABA_A\rho$1 1B	−3.04 ± 0.14	1042	4
GLIC−$GABA_A\rho$1 OB	−2.70 ± 0.03[c]	2061	4
GLIC−Glyα1 1B	−3.36 ± 0.08	456	5
GLIC−Glyα1 0B	−3.53 ± 0.10	327	4

[a]Log IC_{50} values of GLIC−ICD chimeras were compared to those of wild-type GLIC by one-way ANOVA with Dunnett's multiple-comparison post test. Standard Errors are given. [b]Multiplicity-adjusted p value of ≤0.01. [c]Multiplicity-adjusted p value of ≤0.001.

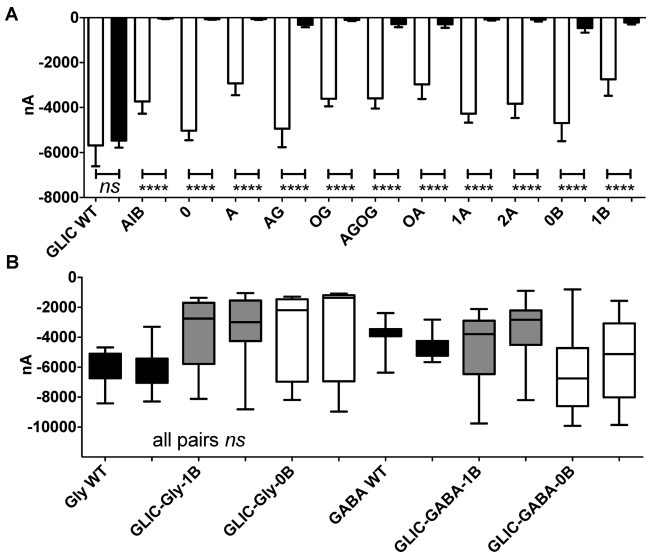

Figure 6. (A) hRIC-3 modulation of plasma membrane expression levels of GLIC−nAChα7−ICD chimeras. Wild-type GLIC and GLIC chimeras were expressed without (white bars with black line) and with hRIC-3 (black bars) in *X. laevis* oocytes, and plasma membrane expression levels were investigated with TEVC after 48 h by switching the pH of the external buffer from 7.5 to 5. RIC-3 co-expression did not alter wild-type GLIC current amplitudes but almost abolished currents induced by application of acidic pH for all functional chimeras. The number of oocytes (n) used for each construct and condition was 5−11. (B) Co-expression of RIC-3 did not alter pLGIC with ICDs from anion-conducting channels for wild-type Glyα1 and $GABA_A\rho$1 (black bars) or the respective chimeras, 1B chimeras (gray bars) or 0B chimeras (white bars). The number of oocytes (n) used for each construct and condition was 10−20. For each construct, the current amplitude without hRIC-3 (left) was compared to that with hRIC-3 (right) with a one-way ANOVA and Holm-Šídák. Significance is indicated as ns (not significant), and multiplicity-adjusted p values are reported as <0.0001 (four asterisks).

proteins was also confirmed by dynamic light scattering experiments, which gave a hydrodynamic radius of 7.6 ± 0.3 nm, and a calculated molecular mass of the protein−detergent complex of 275 ± 23 kDa (n = 10, from two different preparations). Additionally, we microtransplanted purified DDM-solubilized protein into *X. laevis* oocytes (Figure 7D). The oocytes injected with the GLIC−5-HT_{3A}−ICD 1B chimera and uninjected oocytes both displayed currents in response to pH 4.0. However, the responses from the GLIC−5-HT_{3A}−ICD 1B chimera of −90.7 ± 6.2 nA (mean ± SEM; n = 4) at pH 4.0 were ∼3-fold greater (unpaired t test; p = 0.0002) than the current responses observed in uninjected oocytes [−30.1 ± 4.6 nA (mean ± SEM; n = 4)]. The observed weak proton-induced currents, from endogenous acid-sensitive channels, in uninjected oocytes have been reported elsewhere.[36] The functionality of the transplanted GLIC−5-HT_{3A}−ICD 1B chimera in this bulk assay further is comparable to results previously published under similar conditions for GLIC and further substantiates pentameric assembly of the chimera.[36,42]

DISCUSSION

The structure and function of the extracellular and transmembrane domains of pLGICs have been widely investigated in different members of the superfamily. These domains are major determinants of ligand binding, channel gating, and ion permeation. They share significant sequence identities and the same overall fold within different receptor subtypes. On the other hand, the structure and function of the intracellular domain have been far less investigated and are not fully understood. The ICD is known to play a crucial role in assembly, trafficking, and anchoring of Cys-loop receptors.[43,44] It is a target for post-translational modifications like palmitoylation, phosphorylation, and ubiquitination, which can modulate receptor function.[45−47] Additionally, the ICD directly contributes to the modulation of ion flux. For 5-HT_{3A}R, it has been shown previously that arginines in the MA helix limit the single-channel conductance to subpicosiemen levels.[48,49] It was initially presumed that those arginines line intracellular portals that connect the intracellular side to the channel lumen. A recent crystal structure of protease-digested 5-HT_{3A} with a cleaved intracellular domain, however, showed that those arginines are involved in salt bridges with a post M3 loop and are in fact not lining the ion pathway.[28] Interestingly, comparable mutations in other Cys-loop receptors resulted in only minor alterations of single-channel conductance.[50] For anionic GlyR, corresponding mutations in the MA helix have only a weak impact on single-channel conductance,[51] and removal of the entire ICD does not affect the single-channel conductance.[52] Many single-point mutations in pLGIC have been shown to alter single-channel conductance, while the respective positions are distal from the ion conduction pathway. For example, a single-channel proton transfer approach showed changes in single-channel conductance for many positions in M1 and M3 of nAChR.[53] This indicates that more research is necessary to fully understand how the ICD modulates ion flux. The ICD is the most divergent domain with respect to both length (approximately 50−270 amino acids) and amino acid sequence. This diversity makes the ICD an intriguing target for the future design of subunit-specific drugs. However, the diversity in primary sequence and length of the ICD also makes difficult the use of computational approaches to elucidate possible structures of the ICD. As a result, it is essential to study the three-dimensional structure of the ICD for individual members of the superfamily.

In this study, we have used a chimera approach to introduce ICDs from eukaryotic receptors into the prokaryotic GLIC. GLIC is the best-studied prokaryotic pLGIC homologue. Its X-ray structure has been determined with various ligands, and structures of functionally altered mutants have also been determined at high resolution for functional investigations.[22,24,33,54] Chimera approaches have been successfully

DOI: 10.1021/acs.biochem.5b00203
Biochemistry 2015, 54, 2670−2682

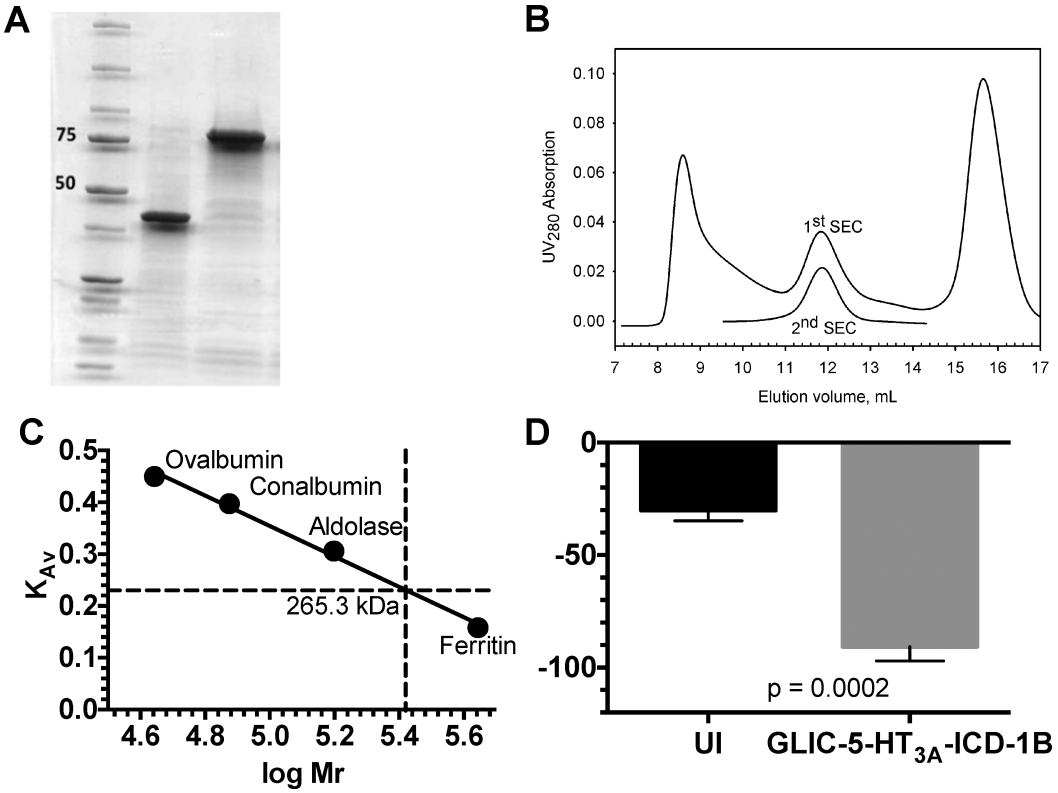

Figure 7. Purification and size exclusion chromatography of the GLIC−5-HT$_{3A}$−ICD 1B chimera from *E. coli*. (A) Protein was purified from *E. coli* membranes, expressing the GLIC−5-HT$_{3A}$−ICD 1B chimera by chromatography on Ni-NTA resin. Eluted protein fractions were resolved on a 4 to 15% polyacrylamide gel (TGX) and stained with Coomassie Blue. The positions of the molecular mass protein markers are indicated in kilodaltons. The left lane contained protein cleaved with HRV 3C protease. Note that PelB−His$_{10}$−MBP (calculated molecular mass of 46 kDa) and GLIC−5-HT$_{3A}$−ICD 1B (calculated molecular mass 49 kDa) run as one broad band because the chimera and MBP are approximately the same size. The right lane contained the eluate from the immobilized metal affinity chromatography (Nickel), PelB−His$_{10}$−MBP−GLIC−5-HT$_{3A}$−ICD 1B (calculated molecular mass of 95 kDa). (B) One milligram of affinity-purified and cleaved protein was loaded on a Superdex 200 10/300 column for size exclusion chromatography (SEC) and resolved in buffer A containing 0.1% DDM (first SEC). Fractions corresponding to the pentameric GLIC−5-HT$_{3A}$−ICD 1B chimera were reloaded into the SEC apparatus (second SEC). A representative example of three independent runs is shown. (C) Calibration and size determination of GLIC−5-HT$_{3A}$−ICD 1B via SEC. $K_{av} = (V_E - V_0)/(V_C - V_0)$, where V_E is the elution volume, V_C is the volume of the column, and V_0 is the void volume. The elution volume of GLIC−5-HT$_{3A}$−ICD 1B indicates a size of 265.3 kDa. (D) Injection of purified GLIC−5-HT$_{3A}$−ICD 1B into *X. laevis* oocytes yielded currents upon switching perfusion buffer from pH 7.5 to 4.0 that were significantly larger than those of uninjected (UI) oocytes.

applied between different eukaryotic pLGIC family members.[31,54−56]

GLIC consists of ECD, TMD, and a short linker between transmembrane segments M3 and M4, in place of the ICD. Previously, we have made a chimera between the mammalian serotonin receptor (5-HT$_{3A}$) and GLIC by replacing the ICD of 5-HT$_{3A}$ with the computationally predicted[16] M3−M4 linker of GLIC (SQPARAA).[40] This 5-HT$_{3A}$glvM3M4 chimera was able to fold, assemble, and function as a ligand-gated ion channel. Interestingly, when the GLIC X-ray structures were published,[19,22] the actual linker between α-helical segments M3 and M4 was shifted and shorter (ESQP, underlined QP was present in both chimera sets). When this linker was used to engineer a 5-HT$_{3A}$−ESQP chimera, it was not functional.[57] Clearly, this indicates that the chimeras that retain function cannot be predicted.

Using the opposite chimera approach, we used the ECD and TMD of GLIC and added the 115-amino acid ICD from 5-HT$_{3A}$, as described in a previous study.[31] For the GLIC−5-HT$_{3A}$−ICD chimera set, we had to vastly modify the insertion points of the ICD and create a total of 12 different chimeras to generate functional constructs. Only two chimeras of 12 were functional proton-gated ion channels in the GLIC−5-HT$_{3A}$−ICD set with pH$_{50}$ values comparable to that of GLIC, whereas the other 10 constructs could not be gated by protons. Here, we have engineered three novel sets of GLIC−eukaryotic−ICD constructs with ICDs nAChα7 (72 amino acids), GABA$_A\rho$1 (82 amino acids), and Glyα1 (75 amino acids) added to the GLIC M3−M4 linker. To optimize the insertion points of the ICD, both the N- and C-terminal regions of GLIC adjacent to the inserted ICD were modified yielding 12 chimeras for each GLIC−eukaryotic−ICD set.

In contrast to this previous set, the vast majority of the chimeras from the GLIC−nAChα7−ICD, GLIC−Glyα1−ICD, and GLIC−GABA$_A\rho$1−ICD sets were functional proton-gated ion channels. We identified 11 functional chimeras in the GLIC−nAChα7−ICD set, 10 in the GLIC−Glyα1−ICD set, and 12 in the GLIC−GABA$_A\rho$1−ICD set, with pH$_{50}$ values only up to 10-fold different from that of GLIC. Therefore, we conclude that the insertion of eukaryotic ICDs into GLIC only moderately interfered with conformational transitions necessary to couple ligand binding to channel gating. Importantly, the functionality also indicates that the insertions allowed the assembly of the chimeras into functional oligomers. Functional

DOI: 10.1021/acs.biochem.5b00203
Biochemistry 2015, 54, 2670−2682

channels have so far been reported only for the pentameric assemblies of this ion channel superfamily; therefore, the functionality of our chimeras likely indicates their pentameric assembly. It is intriguing to speculate why only two 5-HT_{3A} chimeras were functional but significantly more in all other sets. The X-ray structure of the 5-HT_{3A} receptor shows that the MA helix is continuous with the M4 helix. Only the chimeras with the "B" linker between ICD and M4 for this chimera set were functional (0B and 1B), which indicates that significant constraints existed with regard to the insertion of the MA helix in relation to M4. For the N-terminal insertion, both the "0" and "1" insertions lead to functional channels in conjunction with the C-terminal "B". This indicates that there is more flexibility in this post-M3 area. Indeed, the crystal structure shows a flexible linker between M3 and a subsequent short intracellular helix that forms salt bridges with three arginines in the MA helix. It is possible that the other ICDs tested in this study do not have an MA helix that is continuous with M4 or none at all, which would significantly relax steric constraints for making certain linkers work. The differences observed with just the number of functional chimeras in each set already underline the great diversity of the ICDs.

The transmembrane domain of pLGICs is composed of four α-helices, named M1−M4, that form a transmembrane pore bordered by the M2 helices. The flow of ions across the membrane is inhibited by a structurally diverse class of molecules, including tricyclic antidepressants, anesthetics, and quaternary ammonium compounds that bind to the transmembrane pore. TBA as an open channel blocker and quaternary ammonium compound is known to reversibly inhibit GLIC in its open state.[33] TBA is shown to bind at the center, halfway across the membrane. To investigate whether the insertion of the ICD between M3 and M4 altered the transmembrane channel pore in GLIC−eukaryotic−ICD chimeras, we tested the inhibitory effect of TBA on the chimeric channels by TEVC recordings in oocytes. The half-maximal inhibitory concentration (IC_{50}) of TBA was determined for GLIC and for all 1B and 0B chimeras from all four chimera sets. The IC_{50} values between GLIC−ICD chimeras and wild-type GLIC were between 5-fold lower and 4-fold higher. Similar concentration ranges have been reported for similar cationic blockers within the pentameric ligand-gated ion channel family.[33,58−60] The proton and TBA dose−response curves overall indicate that the insertion of the large ICDs is tolerated by the parent GLIC channel.

To assess the folding of the engineered ICDs in functional chimeras, we used the modulation of expression of functional GLIC−eukaryotic−ICD-containing receptors by the chaperone protein RIC-3. Under our experimental conditions, the level of expression of functional GLIC−nAChα7−ICD chimeras but not wild-type GLIC was reduced by co-expression of RIC-3, as determined by reduction of proton-induced currents in TEVC experiments in *X. laevis* oocytes. On the basis of these data, we conclude that the α7 ICD in these chimeras is folded to interact with RIC-3. We did not observe any changes in current amplitudes of oocytes co-expressing RIC-3 and GLIC−Glyα1−ICD or GLIC−$GABA_A\rho$1−ICD chimeras as compared to the chimeras alone. These results are in agreement with previous observations for $GABA_A$, glycine, or glutamate receptors showing that RIC-3 does not affect the expression levels of these receptors.[38,39,41] We have previously shown that RIC-3 can modulate current amplitudes of GLIC−5-HT_{3A}−ICD 1B and 0B chimeras,[31] which confirms that the 5-HT_{3A}−ICD in the chimeras is folded in a native conformation or at least in a conformation that supports interaction with RIC-3. Our data also support the conclusion that the ICD mediates the interaction with RIC-3. We have shown that expression of wild-type 5-HT_{3A}R on oocyte plasma membranes is also inhibited by co-expression of RIC-3 by measuring the maximal 5-HT-inducible current with TEVC.[40] Replacement of the ICD of 5-HT_{3A}R with SQPARAA (5-HT_{3A}-glvM3M4) abolished RIC-3 inhibition, indicating that the ICD is required for the RIC-3 effect.[40]

GLIC and GLIC−5-HT_{3A} 1B and 0B chimeric proteins were expressed in *E. coli* as fusion constructs with N-terminal maltose-binding protein (MBP). We have shown that GLIC−5-HT_{3A} 1B and 0B chimeric proteins can be purified from *E. coli* in quantities and purities amenable to structural studies. It is possible that parts of the 5-HT_{3A}−ICD, likely inside the third that was proteolyzed for determination of the X-ray structure, do not have a defined secondary structure. This may prevent determination of the structure of such segments with X-ray crystallography. However, proteins with long loops of non-defined secondary structure have been crystallized in the past. The structure of the dysferlin inner DysF domain, for example, was determined at a resolution of 1.9 Å despite the presence of several loops, the longest being 77 amino acids in length.[61] Additionally, the chimeras are also valuable tools for other structural methods (EPR and NMR spectroscopy, for example) for obtaining structural information about potential flexible segments.

The pentameric assembly of purified GLIC−5HT_{3A}−ICD 1B receptors in solution was confirmed by light scattering experiments and size exclusion chromatography. Additionally, microtransplantation into oocytes yielded proton-gated channels, further corroborating pentameric assembly. Importantly, this underlines that the pentameric assembly of purified protein is maintained for GLIC−5HT_{3A}−ICD chimeras in solution. Previously, it was shown that the ECD of GLIC alone did not support pentameric assembly in solution.[62] In fact, size exclusion chromatography indicated a monomeric state of GLIC−ECD in solution, even at the high concentrations used for crystallization. Surprisingly, upon crystallization, GLIC−ECD showed a hexameric quaternary structure. On the other hand, acetylcholine-binding protein,[11,12] a non-channel soluble protein found in the snail *Lymnaea stagnalis*, that is homologous to the ECD of nAChR, and engineered ECD-only constructs of pLGIC that can form functional homopentameric pLGIC, including Gly$R\alpha$1 subunits, are pentameric assemblies under comparable conditions in solution.[63] Subunits of nAChRα1 that normally are found in heteropentamers do not assemble into higher oligomeric states.[64] Constructs that solely consist of the TMD are able to pentamerize, as was shown in a multitude of elegant NMR studies, for both homopentameric (nAChα7) and heteropentameric (nAChα4 and β2) pLGICs.[65,66]

Our ultimate goal was to construct GLIC−ICD chimeras with both ICDs from anion-conducting and cation-conducting eukaryotic pLGICs that are both functional as ligand-gated ion channels and additionally retain the homopentameric assembly of GLIC and of pLGIC in general during high-level overexpression in *E. coli* and purification to homogeneity. GLIC−eukaryotic−ICD constructs can be used as valuable tools for obtaining atomic resolution structures of diverse Cys-loop receptor intracellular domains. The chimera approach based on the GLIC backbone with a determined X-ray structure provides the basis for high-level expression and will help in

DOI: 10.1021/acs.biochem.5b00203
Biochemistry 2015, 54, 2670−2682

model building during X-ray structure generation. Importantly, the large quantities of chimeras that can be generated open multiple other avenues for structural studies. Overall, the chimeras may expedite and facilitate elucidation of the expected intrinsic variability in structural folds of the ICD of eukaryotic pLGICs that is intrinsically diverse with regard to both its length and amino acid composition. Additionally, the chimeras provide valuable tools for studying functional contributions, posttranslational modifications, and interacting proteins of the ICD in more detail. This will pave the way for developing structure-based subtype-selective drugs and provide new insights into the understanding of the molecular mechanisms governing Cys-loop receptor function and its modulation by various therapeutic and addictive drugs.

AUTHOR INFORMATION

Corresponding Author

*Department of Cell Physiology and Molecular Biophysics, Center for Membrane Protein Research, School of Medicine, Texas Tech University Health Sciences Center, 3601 4th St., Lubbock, TX 79430. Telephone: +1 806 743 4059. Fax: +1 806 743 1512. E-mail: michaela.jansen@ttuhsc.edu.

Present Address

[@]N.M.: Department of Internal Medicine, Yale University, New Haven, CT 06520-8056.

Author Contributions

N.M. and S.N.N. contributed equally to this study.

Funding

Research reported in this publication was supported by the National Institute of Neurological Disorders and Stroke of the National Institutes of Health via Grant R01NS077114 (to M.J.). Preliminary seed grants were supported by the Center for Membrane Protein Research of the Texas Tech University Health Sciences Center (TTUHSC) (to M.J.), by a South Plains Foundation grant (to M.J.), by a Howard Hughes Medical Institute grant through the Undergraduate Science Education Program to Texas Tech University (to A.A.), and by the TTUHSC School of Medicine Medical Student Summer Research Program (to A.F.N.).

Notes

The authors declare no competing financial interest.

ACKNOWLEDGMENTS

We thank the Texas Tech University Health Sciences Center (TTUHSC) Imaging Facility as some of the images and or data were generated in the Image Analysis Core Facility & Molecular Biology Core Facility supported by TTUHSC.

REFERENCES

(1) Changeux, J. P., Kasai, M., and Lee, C. Y. (1970) Use of a snake venom toxin to characterize the cholinergic receptor protein. *Proc. Natl. Acad. Sci. U.S.A. 67*, 1241−1247.

(2) Boess, F. G., and Martin, I. L. (1992) Purification and characterization of 5-HT3 receptors from NG108-15 neuroblastoma x glioma cells. *Biochem. Soc. Trans. 20*, 217S.

(3) Sigel, E., and Barnard, E. A. (1984) A γ-aminobutyric acid/benzodiazepine receptor complex from bovine cerebral cortex. Improved purification with preservation of regulatory sites and their interactions. *J. Biol. Chem. 259*, 7219−7223.

(4) Pfeiffer, F., Graham, D., and Betz, H. (1982) Purification by affinity chromatography of the glycine receptor of rat spinal cord. *J. Biol. Chem. 257*, 9389−9393.

(5) Picciotto, M. R., Brunzell, D. H., and Caldarone, B. J. (2002) Effect of nicotine and nicotinic receptors on anxiety and depression. *NeuroReport 13*, 1097−1106.

(6) Perry, E. K., Lee, M. L., Martin-Ruiz, C. M., Court, J. A., Volsen, S. G., Merrit, J., Folly, E., Iversen, P. E., Bauman, M. L., Perry, R. H., and Wenk, G. L. (2001) Cholinergic activity in autism: Abnormalities in the cerebral cortex and basal forebrain. *Am. J. Psychiatry 158*, 1058−1066.

(7) Martin, L. F., Kem, W. R., and Freedman, R. (2004) Alpha-7 nicotinic receptor agonists: Potential new candidates for the treatment of schizophrenia. *Psychopharmacology 174*, 54−64.

(8) Maelicke, A., and Albuquerque, E. X. (2000) Allosteric modulation of nicotinic acetylcholine receptors as a treatment strategy for Alzheimer's disease. *Eur. J. Pharmacol. 393*, 165−170.

(9) Kuryatov, A., Gerzanich, V., Nelson, M., Olale, F., and Lindstrom, J. (1997) Mutation causing autosomal dominant nocturnal frontal lobe epilepsy alters Ca^{2+} permeability, conductance, and gating of human α4β2 nicotinic acetylcholine receptors. *J. Neurosci. 17*, 9035−9047.

(10) Picciotto, M. R., Zoli, M., Rimondini, R., Lena, C., Marubio, L. M., Pich, E. M., Fuxe, K., and Changeux, J. P. (1998) Acetylcholine receptors containing the β2 subunit are involved in the reinforcing properties of nicotine. *Nature 391*, 173−177.

(11) Smit, A. B., Brejc, K., Syed, N., and Sixma, T. K. (2003) Structure and function of AChBP, homologue of the ligand-binding domain of the nicotinic acetylcholine receptor. *Ann. N.Y. Acad. Sci. 998*, 81−92.

(12) Sixma, T. K., and Smit, A. B. (2003) Acetylcholine binding protein (AChBP): A secreted glial protein that provides a high-resolution model for the extracellular domain of pentameric ligand-gated ion channels. *Annu. Rev. Biophys. Biomol. Struct. 32*, 311−334.

(13) Brejc, K., van Dijk, W. J., Smit, A. B., and Sixma, T. K. (2002) The 2.7 Å structure of AChBP, homologue of the ligand-binding domain of the nicotinic acetylcholine receptor. *Novartis Found. Symp. 245*, 22−29 , discussion 29−32, 165−168.

(14) Miyazawa, A., Fujiyoshi, Y., and Unwin, N. (2003) Structure and gating mechanism of the acetylcholine receptor pore. *Nature 423*, 949−955.

(15) Unwin, N. (2005) Refined structure of the nicotinic acetylcholine receptor at 4 Å resolution. *J. Mol. Biol. 346*, 967−989.

(16) Tasneem, A., Iyer, L. M., Jakobsson, E., and Aravind, L. (2005) Identification of the prokaryotic ligand-gated ion channels and their implications for the mechanisms and origins of animal Cys-loop ion channels. *Genome Biol. 6*, R4.

(17) Samson, R., Legendre, J. B., Christen, R., Fischer-Le Saux, M., Achouak, W., and Gardan, L. (2005) Transfer of *Pectobacterium chrysanthemi* (Burkholder et al. 1953) Brenner et al. 1973 and *Brenneria paradisiaca* to the genus *Dickeya* gen. nov. as *Dickeya chrysanthemi* comb. nov. and *Dickeya paradisiaca* comb. nov. and delineation of four novel species, *Dickeya dadantii* sp. nov., *Dickeya dianthicola* sp. nov., *Dickeya dieffenbachiae* sp. nov. and *Dickeya zeae* sp. nov. *Int. J. Syst. Evol. Microbiol. 55*, 1415−1427.

(18) Hilf, R. J., and Dutzler, R. (2008) X-ray structure of a prokaryotic pentameric ligand-gated ion channel. *Nature 452*, 375−379.

(19) Hilf, R. J., and Dutzler, R. (2009) Structure of a potentially open state of a proton-activated pentameric ligand-gated ion channel. *Nature 457*, 115−118.

(20) Nury, H., Van Renterghem, C., Weng, Y., Tran, A., Baaden, M., Dufresne, V., Changeux, J. P., Sonner, J. M., Delarue, M., and Corringer, P. J. (2011) X-ray structures of general anaesthetics bound to a pentameric ligand-gated ion channel. *Nature 469*, 428−431.

(21) Corringer, P. J., Baaden, M., Bocquet, N., Delarue, M., Dufresne, V., Nury, H., Prevost, M., and Van Renterghem, C. (2010) Atomic structure and dynamics of pentameric ligand-gated ion channels: New insight from bacterial homologues. *J. Physiol. 588*, 565−572.

(22) Bocquet, N., Nury, H., Baaden, M., Le Poupon, C., Changeux, J. P., Delarue, M., and Corringer, P. J. (2009) X-ray structure of a pentameric ligand-gated ion channel in an apparently open conformation. *Nature 457*, 111−114.

DOI: 10.1021/acs.biochem.5b00203
Biochemistry 2015, 54, 2670−2682

(23) Pan, J., Chen, Q., Willenbring, D., Yoshida, K., Tillman, T., Kashlan, O. B., Cohen, A., Kong, X. P., Xu, Y., and Tang, P. (2012) Structure of the pentameric ligand-gated ion channel ELIC cocrystallized with its competitive antagonist acetylcholine. *Nat. Commun. 3*, 714.
(24) Pan, J., Chen, Q., Willenbring, D., Mowrey, D., Kong, X. P., Cohen, A., Divito, C. B., Xu, Y., and Tang, P. (2012) Structure of the pentameric ligand-gated ion channel GLIC bound with anesthetic ketamine. *Structure 20*, 1463−1469.
(25) Spurny, R., Ramerstorfer, J., Price, K., Brams, M., Ernst, M., Nury, H., Verheij, M., Legrand, P., Bertrand, D., Bertrand, S., Dougherty, D. A., de Esch, I. J., Corringer, P. J., Sieghart, W., Lummis, S. C., and Ulens, C. (2012) Pentameric ligand-gated ion channel ELIC is activated by GABA and modulated by benzodiazepines. *Proc. Natl. Acad. Sci. U.S.A. 109*, E3028−E3034.
(26) Hibbs, R. E., and Gouaux, E. (2011) Principles of activation and permeation in an anion-selective Cys-loop receptor. *Nature 474*, 54−60.
(27) Miller, P. S., and Aricescu, A. R. (2014) Crystal structure of a human GABA receptor. *Nature 512*, 270−275.
(28) Hassaine, G., Deluz, C., Grasso, L., Wyss, R., Tol, M. B., Hovius, R., Graff, A., Stahlberg, H., Tomizaki, T., Desmyter, A., Moreau, C., Li, X. D., Poitevin, F., Vogel, H., and Nury, H. (2014) X-ray structure of the mouse serotonin 5-HT3 receptor. *Nature 512*, 276−281.
(29) Mnatsakanyan, N., and Jansen, M. (2013) Experimental determination of the vertical alignment between the second and third transmembrane segments of muscle nicotinic acetylcholine receptors. *J. Neurochem. 125*, 843−854.
(30) Papke, R. L. (2014) Merging old and new perspectives on nicotinic acetylcholine receptors. *Biochem. Pharmacol. 89*, 1−11.
(31) Goyal, R., Salahudeen, A. A., and Jansen, M. (2011) Engineering a prokaryotic Cys-loop receptor with a third functional domain. *J. Biol. Chem. 286*, 34635−34642.
(32) Olsen, R. W., and Sieghart, W. (2008) International Union of Pharmacology. LXX. Subtypes of γ-aminobutyric acid(A) receptors: Classification on the basis of subunit composition, pharmacology, and function. Update. *Pharmacol. Rev. 60*, 243−260.
(33) Hilf, R. J., Bertozzi, C., Zimmermann, I., Reiter, A., Trauner, D., and Dutzler, R. (2010) Structural basis of open channel block in a prokaryotic pentameric ligand-gated ion channel. *Nat. Struct. Mol. Biol. 17*, 1330−1336.
(34) Miroux, B., and Walker, J. E. (1996) Over-production of proteins in *Escherichia coli*: Mutant hosts that allow synthesis of some membrane proteins and globular proteins at high levels. *J. Mol. Biol. 260*, 289−298.
(35) Pandhare, A., Hamouda, A. K., Staggs, B., Aggarwal, S., Duddempudi, P. K., Lever, J. R., Lapinsky, D. J., Jansen, M., Cohen, J. B., and Blanton, M. P. (2012) Bupropion binds to two sites in the *Torpedo* nicotinic acetylcholine receptor transmembrane domain: A photoaffinity labeling study with the bupropion analogue [(^{125})I]-SADU-3−72. *Biochemistry 51*, 2425−2435.
(36) Labriola, J. M., Pandhare, A., Jansen, M., Blanton, M. P., Corringer, P. J., and Baenziger, J. E. (2013) Structural sensitivity of a prokaryotic pentameric ligand-gated ion channel to its membrane environment. *J. Biol. Chem. 288*, 11294−11303.
(37) Bocquet, N., Prado de Carvalho, L., Cartaud, J., Neyton, J., Le Poupon, C., Taly, A., Grutter, T., Changeux, J. P., and Corringer, P. J. (2007) A prokaryotic proton-gated ion channel from the nicotinic acetylcholine receptor family. *Nature 445*, 116−119.
(38) Halevi, S., McKay, J., Palfreyman, M., Yassin, L., Eshel, M., Jorgensen, E., and Treinin, M. (2002) The *C. elegans* ric-3 gene is required for maturation of nicotinic acetylcholine receptors. *EMBO J. 21*, 1012−1020.
(39) Halevi, S., Yassin, L., Eshel, M., Sala, F., Sala, S., Criado, M., and Treinin, M. (2003) Conservation within the RIC-3 gene family. Effectors of mammalian nicotinic acetylcholine receptor expression. *J. Biol. Chem. 278*, 34411−34417.
(40) Jansen, M., Bali, M., and Akabas, M. H. (2008) Modular design of Cys-loop ligand-gated ion channels: Functional 5-HT3 and GABA ρ1 receptors lacking the large cytoplasmic M3M4 loop. *J. Gen. Physiol. 131*, 137−146.
(41) Wang, Y., Yao, Y., Tang, X. Q., and Wang, Z. Z. (2009) Mouse RIC-3, an endoplasmic reticulum chaperone, promotes assembly of the α7 acetylcholine receptor through a cytoplasmic coiled-coil domain. *J. Neurosci. 29*, 12625−12635.
(42) Dellisanti, C. D., Ghosh, B., Hanson, S. M., Raspanti, J. M., Grant, V. A., Diarra, G. M., Schuh, A. M., Satyshur, K., Klug, C. S., and Czajkowski, C. (2013) Site-directed spin labeling reveals pentameric ligand-gated ion channel gating motions. *PLoS Biol. 11*, e1001714.
(43) Vithlani, M., Terunuma, M., and Moss, S. J. (2011) The dynamic modulation of GABA(A) receptor trafficking and its role in regulating the plasticity of inhibitory synapses. *Physiol. Rev. 91*, 1009−1022.
(44) Tretter, V., Jacob, T. C., Mukherjee, J., Fritschy, J. M., Pangalos, M. N., and Moss, S. J. (2008) The clustering of GABA(A) receptor subtypes at inhibitory synapses is facilitated via the direct binding of receptor α2 subunits to gephyrin. *J. Neurosci. 28*, 1356−1365.
(45) Papke, D., and Grosman, C. (2014) The role of intracellular linkers in gating and desensitization of human pentameric ligand-gated ion channels. *J. Neurosci. 34*, 7238−7252.
(46) Swope, S. L., Moss, S. I., Raymond, L. A., and Huganir, R. L. (1999) Regulation of ligand-gated ion channels by protein phosphorylation. *Adv. Second Messenger Phosphoprotein Res. 33*, 49−78.
(47) Baptista-Hon, D. T., Deeb, T. Z., Lambert, J. J., Peters, J. A., and Hales, T. G. (2013) The minimum M3-M4 loop length of neurotransmitter-activated pentameric receptors is critical for the structural integrity of cytoplasmic portals. *J. Biol. Chem. 288*, 21558−21568.
(48) Kelley, S. P., Dunlop, J. I., Kirkness, E. F., Lambert, J. J., and Peters, J. A. (2003) A cytoplasmic region determines single-channel conductance in 5-HT3 receptors. *Nature 424*, 321−324.
(49) Peters, J. A., Kelley, S. P., Dunlop, J. I., Kirkness, E. F., Hales, T. G., and Lambert, J. J. (2004) The 5-hydroxytryptamine type 3 (5-HT3) receptor reveals a novel determinant of single-channel conductance. *Biochem. Soc. Trans. 32*, 547−552.
(50) Hales, T. G., Dunlop, J. I., Deeb, T. Z., Carland, J. E., Kelley, S. P., Lambert, J. J., and Peters, J. A. (2006) Common determinants of single channel conductance within the large cytoplasmic loop of 5-hydroxytryptamine type 3 and α4β2 nicotinic acetylcholine receptors. *J. Biol. Chem. 281*, 8062−8071.
(51) Carland, J. E., Cooper, M. A., Sugiharto, S., Jeong, H. J., Lewis, T. M., Barry, P. H., Peters, J. A., Lambert, J. J., and Moorhouse, A. J. (2009) Characterization of the effects of charged residues in the intracellular loop on ion permeation in α1 glycine receptor channels. *J. Biol. Chem. 284*, 2023−2030.
(52) Moroni, M., Biro, I., Giugliano, M., Vijayan, R., Biggin, P. C., Beato, M., and Sivilotti, L. G. (2011) Chloride ions in the pore of glycine and GABA channels shape the time course and voltage dependence of agonist currents. *J. Neurosci. 31*, 14095−14106.
(53) Cymes, G. D., and Grosman, C. (2008) Pore-opening mechanism of the nicotinic acetylcholine receptor evinced by proton transfer. *Nat. Struct. Mol. Biol. 15*, 389−396.
(54) Duret, G., Van Renterghem, C., Weng, Y., Prevost, M., Moraga-Cid, G., Huon, C., Sonner, J. M., and Corringer, P. J. (2011) Functional prokaryotic-eukaryotic chimera from the pentameric ligand-gated ion channel family. *Proc. Natl. Acad. Sci. U.S.A. 108*, 12143−12148.
(55) Bouzat, C., Bren, N., and Sine, S. M. (1994) Structural basis of the different gating kinetics of fetal and adult acetylcholine receptors. *Neuron 13*, 1395−1402.
(56) Eertmoed, A. L., and Green, W. N. (1999) Nicotinic receptor assembly requires multiple regions throughout the gamma subunit. *J. Neurosci. 19*, 6298−6308.
(57) McKinnon, N. K., Bali, M., and Akabas, M. H. (2012) Length and amino acid sequence of peptides substituted for the 5-HT3A receptor M3M4 loop may affect channel expression and desensitization. *PLoS One 7*, e35563.

DOI: 10.1021/acs.biochem.5b00203
Biochemistry 2015, 54, 2670−2682

(58) Kooyman, A. R., Zwart, R., and Vijverberg, H. P. (1993) Tetraethylammonium ions block 5-HT3 receptor-mediated ion current at the agonist recognition site and prevent desensitization in cultured mouse neuroblastoma cells. *Eur. J. Pharmacol. 246*, 247−254.
(59) Charnet, P., Labarca, C., Leonard, R. J., Vogelaar, N. J., Czyzyk, L., Gouin, A., Davidson, N., and Lester, H. A. (1990) An open-channel blocker interacts with adjacent turns of α-helices in the nicotinic acetylcholine receptor. *Neuron 4*, 87−95.
(60) Blanchet, C., and Dulon, D. (2001) Tetraethylammonium ions block the nicotinic cholinergic receptors of cochlear outer hair cells. *Brain Res. 915*, 11−17.
(61) Sula, A., Cole, A. R., Yeats, C., Orengo, C., and Keep, N. H. (2014) Crystal structures of the human Dysferlin inner DysF domain. *BMC Struct. Biol. 14*, 3.
(62) Nury, H., Bocquet, N., Le Poupon, C., Raynal, B., Haouz, A., Corringer, P. J., and Delarue, M. (2010) Crystal structure of the extracellular domain of a bacterial ligand-gated ion channel. *J. Mol. Biol. 395*, 1114−1127.
(63) Liu, Z., Ramanoudjame, G., Liu, D., Fox, R. O., Jayaraman, V., Kurnikova, M., and Cascio, M. (2008) Overexpression and functional characterization of the extracellular domain of the human α1 glycine receptor. *Biochemistry 47*, 9803−9810.
(64) Dellisanti, C. D., Yao, Y., Stroud, J. C., Wang, Z. Z., and Chen, L. (2007) Crystal structure of the extracellular domain of nAChR α1 bound to α-bungarotoxin at 1.94 Å resolution. *Nat. Neurosci. 10*, 953−962.
(65) Bondarenko, V., Mowrey, D., Tillman, T., Cui, T., Liu, L. T., Xu, Y., and Tang, P. (2012) NMR structures of the transmembrane domains of the α4β2 nAChR. *Biochim. Biophys. Acta 1818*, 1261−1268.
(66) Bondarenko, V., Mowrey, D. D., Tillman, T. S., Seyoum, E., Xu, Y., and Tang, P. (2014) NMR structures of the human α7 nAChR transmembrane domain and associated anesthetic binding sites. *Biochim. Biophys. Acta 1838*, 1389−1395.

DOI: 10.1021/acs.biochem.5b00203
Biochemistry 2015, 54, 2670−2682